Environmental Pollution 337 (2023) 122557

Contents lists available at ScienceDirect

Environmental Pollution

journal homepage: www.elsevier.com/locate/envpol

Silver isotopes: A tool to trace smelter-derived contamination☆

Aleš Vaněk [a,*], Maria Vaňková [b], Martin Mihaljevič [b], Vojtěch Ettler [b], Petr Drahota [b], Lenka Vondrovicová [b], Petra Vokurková [a], Ivana Galušková [a], Tereza Zádorová [a], Ryan Mathur [c]

[a] Department of Soil Science and Soil Protection, Faculty of Agrobiology, Food and Natural Resources, Czech University of Life Sciences Prague, Kamýcká 129, 165 00, Prague 6, Czech Republic
[b] Institute of Geochemistry, Mineralogy and Mineral Resources, Faculty of Science, Charles University, Albertov 6, 128 00, Prague 2, Czech Republic
[c] Department of Geology, Juniata College, Huntingdon, PA, 16652, USA

ARTICLE INFO

Keywords:
Smelting
Metallurgy
Ore
Slag
Isotopic fractionation

ABSTRACT

Here, for the first time, we report the concentrations and isotopic data of Ag in a variety of ore and metallurgical samples and forest soils that have been polluted due to Ag–Pb smelter emissions. Similar to the Ag concentrations, we identified a large range of δ^{109}Ag values (from −0.8 to +2.4‰), a ~3‰ spread, within the primary and secondary materials (i.e., galena, fly ash, slag and matte). This phenomenon, however, is evidently unrelated to Ag isotopic fractionation during the smelting process, but it reflects the starting ^{109}Ag/^{107}Ag signal in ore mineral and/or the specific type of ore genesis. The two studied soil profiles differed in Ag isotopic composition, but on the other hand, they consistently showed significantly lighter Ag (≤+0.8‰) of metallurgical origin in the upper horizons compared to the bottom horizons and bedrocks, with low Ag amounts depleted of ^{107}Ag (≤+2.9‰). This isotopic pattern can be attributed to a ternary mixing relationship involving two major anthropogenic Ag components and a minor contribution from geogenic Ag. Accordingly, we did not observe any post-depositional isotopic fractionation in our soils, since Ag was geochemically stable and it was not subjected to leaching. In summary, the Ag isotopes have a potential to trace variations in anthropogenic phases, to monitor specific geochemical processes, and are clearly applicable as anthropogenic Ag source and Ag load proxies.

1. Introduction

Silver (Ag) is a trace element included in the US EPA list of priority pollutants. The toxicity of dissolved Ag species to microbes, viruses and potentially to higher organisms is well known, and it reflects an active (inhibitory) role of Ag^+ in specific biochemical reactions (Fabrega et al., 2011; Nowack et al., 2011; Zhang et al., 2017). Historically, most anthropogenic Ag has been introduced into the environment directly via various wastes from mining and processing of Ag-containing ores, followed by industrial operations (cement production, chemical and energy coal-based industries etc.) (Purcell and Peters, 1998). Post-depositional remobilization of Ag-rich wastes and soils/sediments clearly represents another source of Ag in the environment. More recently, (last ~100 years), the anthropogenic Ag flux has increased due to widespread use of nanoparticle/colloidal Ag (nano-Ag^0), mostly owing to demand for its bactericidal effect and associated applications (Fabrega et al., 2011).

The average Ag concentrations in the upper continental crust and in uncontaminated soils are ~0.05 ppm and ≤0.01–0.1 ppm, respectively (Taylor and McLennan, 1985; Reimann and Fabian, 2022), and can far exceed 1 ppm in areas that have been affected by Ag mining/processing (Ash et al., 2014). Waste materials from Ag pre-concentration or primary Ag metallurgy (post-flotation waste, fly ash, slag etc.) contain up to tens or hundreds of ppm Ag (Scheinert et al., 2009). Since Ag is a highly reactive element, both bulk metal Ag and nano-Ag^0 can readily be transformed into oxidized Ag(I) species (e.g., Ag^+, $AgCl_x^{(x-1)-}$, Ag_2S and Ag_2O) in water-saturated geosystems (Nowack et al., 2011; Zhang et al., 2017) and Ag^+ can even form complexes with organic ligands (Settimio et al., 2015). Furthermore, Ag^+ can be captured by various secondary Fe/Mn-oxides such as goethite (α-FeOOH) and birnessite (δ-MnO_2), specific clay minerals or S-rich humic substances that can be present in soils (Jacobson et al., 2005a,b; Pei et al., 2013; Mathur et al., 2018). Therefore, chemical factors such as soil pH, Eh, phase composition, organic matter quality/content etc., all can influence the alteration of

☆ This paper has been recommended for acceptance by Hefa Cheng.

* Corresponding author.
E-mail address: vaneka@af.czu.cz (A. Vaněk).

https://doi.org/10.1016/j.envpol.2023.122557
Received 25 May 2023; Received in revised form 23 August 2023; Accepted 12 September 2023
Available online 14 September 2023

anthropogenic Ag and its fate in Ag cycle(s).

High-precision determination of Ag stable isotope ratios ($^{109}Ag/^{107}Ag$) has recently been used for the analysis of geological (e.g., Woodland et al., 2005; Schönbachler et al., 2007, 2008; Luo et al., 2010; Guo et al., 2017; Mathur et al., 2018; Fujii and Albarede, 2018; Arribas et al., 2020) and archeological samples, i.e., for the primary Ag-source identification (e.g., Desaulty et al., 2011; Desaulty and Albarède, 2013; Albarède et al., 2016; Fujii and Albarede, 2018; Eshel et al., 2022), but so far has been scarcely used in environmental applications (Lu et al., 2016; Zhang et al., 2017). Probably the best described causes and mechanisms of Ag isotopic fractionation are closely related to the fields of economic geology that deal with the formation or the alteration of specific Ag phases during ore genesis (Anderson et al., 2019; Milot et al., 2022). On the other hand, there are several individual aspects that still remain unknown or unresolved. For example, no study devoted to the isotopic tracing of Ag during the high-T processes (e.g. ore smelting and coal burning) or during its fate in contaminated soils/sediments is available in the literature. Consequently, information of the degree to which Ag can isotopically fractionate during soil sorption, redox reactions, plant uptake etc., relative to its primary source (ore) is also missing. All these data are clearly required before the Ag isotopic signal is accepted as a suitable proxy for understanding Ag deposition, accumulation or fixation mechanisms.

This paper reports the concentration and the isotopic data of Ag from a set of various ore and metallurgical samples and forest soils that have been polluted by Ag–Pb smelter emissions (Příbram, Czech Rep.). We attempted to reveal (i) the changes and variability of Ag isotopic compositions over a local Ag cycle, (ii) anthropogenic versus geogenic Ag inputs in soils and (iii) the post-depositional soil chemistry of Ag that can potentially be associated with the isotopic effects. Leaving this study aside, these data also have relevance to further applying Ag isotopes, i.e., the fate of engineered Ag-nanoparticles in soils, sediments and (waste)water systems.

2. Experimental

2.1. Study area, soil sampling and characterization

The area of Příbram (situated ~60 km SW of Prague, Czech Rep.) has a long-term history of Ag and Pb mining and smelting (Fig. S1, Supplementary Material). The processing of Ag and Pb ores, mainly Ag-containing galena (PbS) (Ettler et al., 2001), has led to environmental contamination. The Příbram smelter has been operational for more than 200 years and in the last ~50 years only Pb-rich wastes, mostly car batteries, have been processed here. However, until the 1930s, the major product of this plant was Ag, after which the production of Pb gradually became more important. In general, historical smelter emissions are thought to be the source responsible for high concentrations of metals/metalloids in local soils; Pb exceeds 10,000 ppm in some cases (Rieuwerts et al., 1999; Ettler et al., 2004, 2005a). It is important to note that the first measurements of pollutant emissions started in the 1960s, and for instance, the annual Pb flux from the smelter accounted for 624 t in 1969. After the installation of modern dust removal system(s) in 1983, the emission loads gradually decreased, and from 1996 they were systematically lower than 3 t Pb/year (Kunický and Vurm, 2011). Although, the total amount of Ag being emitted in the area is unclear, a comparable trend with historical dust/Pb emissions is hypothesized. To comment briefly on the forest management, Norway spruce (*Picea abies* L.) represented the prevailing tree species at the study sites, though currently there is a need for their cutting due to bark beetle damage. For the Ag source tracing, local anthropogenic and natural materials were used in this study: (i) samples of galena, (ii) historical slags and matte, (iii) modern fly ash and (iv) bedrocks, considered to reflect the isotopic compositions of potential Ag endmembers. Detailed chemical and mineralogical data of individual metallurgical samples are available in Ettler et al. (2003, 2005b, 2009a,b).

Two profiles of forest soils (1 and 2) were sampled at two sampling sites as a function of background geology, distance from the smelter and prevailing wind direction in the area (Fig. S1). Cambrian greywackes and conglomerates formed bedrocks in profile 1. In contrast, heterogeneous volcano-sedimentary (Proterozoic) rock was identified in profile 2 (Fig. S1). Individual soils were collected from 1 × 1 m-wide pits according to the natural development of soil horizons. Both profiles, being relatively shallow, were classified as Dystric Cambisols (World Reference Base for Soil Resources, 2006). The soil samples were air-dried, homogenized and sieved through a 2-mm stainless-steel sieve prior to further use or analyses. Selected physicochemical properties are shown in Table 1 and were determined using the following methods. Soil pH was measured at a 1:2 (v/v) ratio of soil and deionized H_2O after 1 h of agitation (Handylab pH-meter, Schott, Germany). The amounts of total organic carbon (TOC), and sulfur (S_{tot}) were determined by catalytic oxidation (1350 °C) using a combination of Metalyt CS 500 and Metalyt CS 530 (ELTRA, Germany) elemental analyzers. The cation exchange capacity (CEC) was determined as a sum of basic cations and Al extracted with 0.1 M $BaCl_2$ solution (ISO 11260:1994) (Standard of Soil Quality, 1994). An acid oxalate extraction (0.2 M ammonium oxalate/oxalic acid at pH 3), according to Pansu and Gautheyrou (2006), was used to reveal the approximate abundance of poorly-crystalline Fe/Mn-oxides and the associated Ag concentration in soil. The exchangeable Ag fraction in soil, corresponding to weakly bound Ag, was determined using a single extraction with 1 M NH_4NO_3 at a 1:2.5 (s/l) ratio (ISO, 19730:2008) (Standard of Soil Quality, 2009). The clay content was measured by the hydrometer method in selected horizons with a low organic matter content (Gee and Bauder, 1986). The X-ray diffraction analysis (XRD), used for soil mineral identification, was performed using an X'Pert Pro diffractometer (PANalytical, the Netherlands) under the following conditions: CuKα radiation, 40 kV, 30 mA, step scanning at 0.02°/150 s in the range 3-70° 2θ.

Prior to determining Ag/element concentrations and Ag stable isotope ratios, soil, bedrock and metallurgical samples were first ground in an agate mill (Pulverisette 0, Fritsch, Germany). Subsequently, a mass of 0.2–0.5 g of each material was decomposed using a hot acid mixture in a microwave unit (Multiwave 5000, Anton Paar, Austria). A solution of concentrated HNO_3 and HF (Merck Ultrapure, Germany) mixed in the ratio of 2:1 was used in a total volume of ≤20 mL, the dissolved sample was subsequently transferred into PTFE beakers (Savillex, USA) and evaporated on a hot plate. The solution residuum was dissolved in 2% HNO_3 and stored for further use. The standard reference materials (SRM) NIST 2710a, 2711a (Montana I/II Soil) and NIST 2782 (Industrial Sludge) were used for the QC of quantitative analyses (Table S1).

2.2. Element concentrations

Silver, Pb, Zn, Cu, Cd, Fe, Mn, Al and Ti concentrations in the total digests of soil, bedrock, PbS and metallurgical samples and in individual soil extracts were determined using either a quadrupole-based inductively coupled plasma mass spectrometer (Q-ICP-MS, iCAP RQ, Thermo Scientific, Germany) or an inductively coupled plasma optical emission spectrometer (ICP-OES, iCAP 6500, Thermo Scientific, UK) under standard analytical conditions. The Ag recoveries for individual SRM are provided in Table S1; the recovery rates varied between 90 and 100% of the certified element concentrations.

2.3. Silver separation

Silver was isolated from the dissolved sample matrix according to the modified chromatographic 2-stage separation method of Schönbachler et al. (2007, 2008). The method is based on the retention of a negatively charged $AgCl_x$ complex onto an exchange resin. The corresponding sample aliquot was evaporated to complete dryness and redissolved in 50 mL 0.5 M HCl so that 100–150 ppb Ag in 3–5 mL (≤750 ng Ag) was then available for each isotopic measurement. The chromatographic

Table 1
Selected physicochemical properties of the studied soil profiles.

Soil profile	Horizon (depth, cm)	Clay (%)	pH	TOC (%)[a]	CEC (cmol/kg)	$S_{tot.}$ (%)[a]	Oxalate-extractable (g/kg)[a]		
							Fe	Al	Mn
1.	O1 (1–3)	–	4.03	45.3	16.3	0.18	1.67	0.76	0.35
	O2 (3–7)	–	3.70	44.9	15.3	0.19	2.40	1.11	0.19
	O3 (7–9)	–	3.70	38.9	19.2	0.16	4.20	2.70	0.17
	AC (9+)	–	3.39	2.81	7.4	0.02	4.10	1.43	0.27
2.	O1 (1–3)	–	3.67	41.6	19.5	0.24	5.32	1.08	0.90
	O2 (3–6)	–	3.45	36.5	21.4	0.38	8.82	1.46	0.31
	O3 (6–9)	–	3.40	30.6	27.5	0.19	4.94	2.97	0.22
	AC (9+)	8.9	3.50	1.68	6.5	<DL	2.56	1.24	0.20

–: not determined; <DL: below the detection limit.
[a] Average values (n = 3).

chemistry utilized new poly-prep 10-mL columns (Bio-Rad, USA) filled with 2 mL of resin (Bio-Rad AG-1X8, 100–200 mesh, Cl^- cycle), followed by steps with reagent mixtures and volumes as follows: (i) 5 × 5 mL of 0.5 M HCl – resin cleaning and treatment; (ii) 10 × 5 mL (0.5 M HCl) – sample loading; (iii) 10 × 5 mL 0.1 M HCl – matrix elution (1); (iv) 10 × 5 mL 0.01 M HCl – matrix elution (2); (v) 10 × 5 mL 0.5 M HNO_3 – Ag fraction elution (50 mL). The obtained samples were evaporated and redissolved in 50 mL 0.5 M HCl. The whole process was repeated to ensure samples with minimum/no matrix effects potentially linked with Ag isotope determination.

It should be noted that the total Ag amount in solutions containing Cl^- is limited by the solubility product of AgCl, where the Ksp = $10^{-10.48}$. Given that the normality of dilute HCl loaded onto the column is 50 mL at 0.5 M, the total activity of Cl^- in solution limits the amount of Ag that could potentially dissolve into solution. Approximately 20 μg of Ag in the salts is the maximum amount of Ag that can dissolve. Since the activity of Ag is controlled by the ionic strength of the solution, the presence of other ions in solution increases the amount of Ag that will be dissolved (Mathur et al., 2018).

Once the final Ag fraction was obtained, the sample was evaporated and diluted in 2% HNO_3. The Ag recoveries were monitored over the whole separation using Q-ICP-MS; they were systematically >95%, avoiding Ag isotopic fractionation during sample purification. Chemicals of ultrapure quality (Merck, Germany) and deionized water (Milli-Q+, Millipore, USA) were used.

2.4. Silver isotope measurement

The determination of $^{109}Ag/^{107}Ag$ ratios, reported as $\delta^{109}Ag$ relative to NIST SRM 978a (Eq. (1)), was performed using a multi-collector inductively coupled plasma mass spectrometer (MC-ICP-MS, Neptune Plus, Thermo Scientific, Germany) equipped with a cyclonic spray chamber and a PFA nebulizer (ESI, Omaha, NE). The instrumental mass bias drift was corrected by a combination of standard-sample bracketing (NIST SRM 978a) and simultaneous measurement of the certified palladium (Pd) isotope standard (NIST SRM 3138; $^{108}Pd/^{105}Pd$ ratio = 1.18899) (Woodland et al., 2005). The solutions containing ~100 ppb Ag were doped with Pd (NIST SRM 3138) to obtain the Ag/Pd ratio 1/2 or 1/3. The cup configuration was as follows: ^{105}Pd-L2, ^{106}Pd-L1, ^{107}Ag–C, ^{108}Pd–H1, ^{109}Ag–H2, and ^{111}Cd–H3. All solutions were measured in 3 blocks of 20 cycles with the integration time 4.194 s.

$$\delta^{109}Ag\ (‰) = \frac{^{109}Ag/^{107}Ag_{sample} - {}^{109}Ag/^{107}Ag_{NIST978a}}{^{109}Ag/^{107}Ag_{NIST978a}} \times 1000 \quad (1)$$

The CRM Astasol AN79001 (Analytika®), set as our in-house standard, was regularly measured between samples and reproduced at $\delta^{109}Ag$ = 0.04‰ (n = 6). The total procedural chemistry blank was <280 pg Ag. All reported isotopic data in this study are assigned an estimated error of ±0.10‰ (2σ). This uncertainty, being achieved in our lab, is based on the reproducibility of complete repeat analyses of NIST SRM 2782 (n = 6) and native Ag (Jáchymov, Czech Rep.) (n = 3) (Table S2). Therefore, it accounts for all possible sources of error – sample dissolution, Ag ion exchange chemistry and mass spectrometry. All isotopic measurements were performed in the laboratories of Isotope Research Center of the Faculty of Science (Charles University, Prague).

3. Results and discussion

3.1. Silver in metallurgical materials

Silver concentrations in the studied metallurgical samples were relatively low (1-68 mg/kg). In contrast, galena samples showed a wide range of Ag concentrations (15-4100 mg/kg), indicating its formation over several generations with varying amounts of available Ag (Table 2). Comparison of Ag concentrations in the fly ash (A1) and the slag (56A) collected in the early 1980s suggests that the latter is depleted of Ag. This finding points to a tendency of Ag to preferentially enter metal and gas phases over a "glassy" slag phase during pyrometallurgical processes (Nakajima et al., 2010, 2011). As for Cu smelting, for example, Nakajima et al. (2011) report that the thermodynamic parameters of Ag generally result in the increased solubility and accumulation of dissolved Ag species in the metal Cu melt, thus a resulting depletion of Ag in the residual slag phase. As far as the Ag concentrations in the medieval/old slags are concerned (9–18 mg/kg), obviously, we do not have accurate Ag data about smelter feeds, source ore minerals, or fly ashes to be able to evaluate Ag loads during historical Ag smelting at Příbram. However, there is plenty of evidence for a lower efficacy of old smelting technologies that can be responsible for higher Ag amounts in both slag and matte materials (Ettler et al., 2009a,b), which is in agreement with e.g. contrasting Ag proportions between the modern slag and the fly ash.

Silver isotopic compositions (in $\delta^{109}Ag$) of galena and metallurgical samples varied significantly, from −0.76 to +2.38‰ (Fig. 1). Regarding the comparison of individual slags only, the samples were variable too, and ranged from +1.37 to +2.32‰ (n = 4) (Table 2). The isotopic signatures for slags can therefore reflect differences in starting ore material, complex slag mineralogy (Ettler et al., 2003, 2009a) or even the type of slag production (medieval versus ≤200-years-old technologies). Although no Ag isotope data are available for historical smelter charges with different Pb/Ag ratios, the variable Ag isotopic signatures in the galena samples (between −0.76 and + 0.13‰) combined with very heavy slags (≤+2.32‰) (Fig. 1) suggest that some Ag may come from other phases with contrasting $^{109}Ag/^{107}Ag$ ratios. For example, native Ag, various types of Ag-bearing sulphides and sulfosalts have been detected in Příbram ores and slags (Ettler et al., 2009a,b). Moreover, recent findings by Wang et al. (2022) and Milot et al. (2022) even illustrate a large isotopic variability of Ag in PbS (≤6‰) within individual polymetallic systems, suggesting a sequence of PbS formation with markedly different isotopic compositions. It is important to note that the Ag isotopic variability in metallurgical waste products tends to reflect phase compositions of the processed materials, ores, thus being capable to overprint the isotopic fractionation during Ag evaporation

Table 2
Total, exchangeable and oxalate-extractable concentrations of Ag (and Pb), Ag isotopic compositions (expressed as δ^{109}Ag relative to NIST SRM 978a) and Ag/Ti ratios and τ-values in the studied soil, bedrock, galena and metallurgical samples – historical and modern slags, matte and fly ashes.

Soil profile/sample	Horizon	Total Ag (mg/kg)	Total Pb (mg/kg)	Exchangeable Ag (μg/kg)	O.-extractable Ag (μg/kg)	δ^{109}Ag (‰)	Ag/Ti (× 10^3)	τ-value
1.	O1	2.13 ± 0.02	2900 ± 40	2.25	<DL	+0.796	2.59	24
	O2	5.45 ± 0.07	7990 ± 50	6.47	4.71	+0.436	5.55	52
	O3	5.17 ± 0.06	6840 ± 30	6.78	4.96	+0.497	3.52	32
	AC	1.04 ± 0.32	347 ± 1	<DL	<DL	+1.939	0.22	1
	bedrock 1	0.21 ± 0.17	19 ± 3	–	–	+1.572	0.11	–
2.	O1	13.7 ± 0.51	12,000 ± 90	10.9	13.5	−0.028	10.3	153
	O2	26.8 ± 0.8	27,900 ± 400	13.8	53.4	−0.045	17.3	260
	O3	11.9 ± 0.2	7500 ± 50	6.46	15.4	+0.095	5.74	85
	AC	1.79 ± 0.23	916 ± 3	1.96	<DL	+0.700	0.39	5
	bedrock 2	0.17 ± 0.13	102 ± 4	–	–	+2.912	0.07	–
galena (1327)[e]		14.9 ± 0.5	~750,000	–	–	−0.759	–	–
galena (GVA1)[e]		~792	~820,000	–	–	−0.025	–	–
galena (GVA2)[e]		~4105	~870,000	–	–	+0.113	–	–
galena (GVA3)[e]		~3962	~860,000	–	–	−0.002	–	–
galena (GVA8)[e]		~610	~900,000	–	–	−0.379	–	–
galena (GVA10)[e]		~1947	~880,000	–	–	+0.125	–	–
medieval slag, ore processing (B14)[a]		18.4 ± 0.6	~140,000	–	–	+1.366	6.16	–
medieval slag, ore processing (B22)[a]		9.49 ± 0.22	~221,000	–	–	+2.323	3.22	–
medieval slag, ore processing (B25)[a]		14.4 ± 0.1	~171,000	–	–	+1.845	5.05	–
old slag, 150–200 years, ore processing (30A)[b]		15.9 ± 0.1	~18,900	–	–	+2.190	–	–
modern slag, battery processing, 1980s (56A)[b]		1.0 ± 0	~15,800	–	–	–	–	–
old matte, 150–200 years, ore processing (72C)[c]		13.8 ± 0.4	~58,800	–	–	+0.249	–	–
modern fly ash, battery processing, year 1982 (A1)[d]		68.0 ± 3.0	~135,000	–	–	+2.381	–	–
modern fly ash, battery processing, year 2002 (A3)[d]		1.44 ± 0.22	~368,000	–	–	–	–	–
modern fly ash, battery processing, year 2002 (A3-B)[d]		0.9 ± 0	~41,300	–	–	–	–	–

–: not determined; <DL: below the detection limit; O.-extractable: oxalate-extractable.
The uncertainties for total Ag and Pb concentrations in soil and metallurgical samples are reported at the 1σ level (n = 3).
The δ^{109}Ag values are assigned an error of ±0.10‰ (2σ) that is based on the reproducibility of complete repeat analyses (n = 6) of NIST SRM 2782 (Table S2).
The τ parameter was calculated as follows: (Ag/Ti)soil/(Ag/Ti)bedrock – 1; τ > 0 indicates Ag enrichment.
The 56A, A3 and A3-B samples (modern slag and fly ashes) could not be analyzed for Ag stable isotope ratios due to the post-separation matrix effects.
For more details.
[a] Ettler et al. (2009a).
[b] Ettler et al. (2003).
[c] Ettler et al. (2009b).
[d] Ettler et al. (2005b).
[e] Samples provided by the Mineralogical museum or originating from the ore collections of the Charles University (Prague, Czech Rep.).

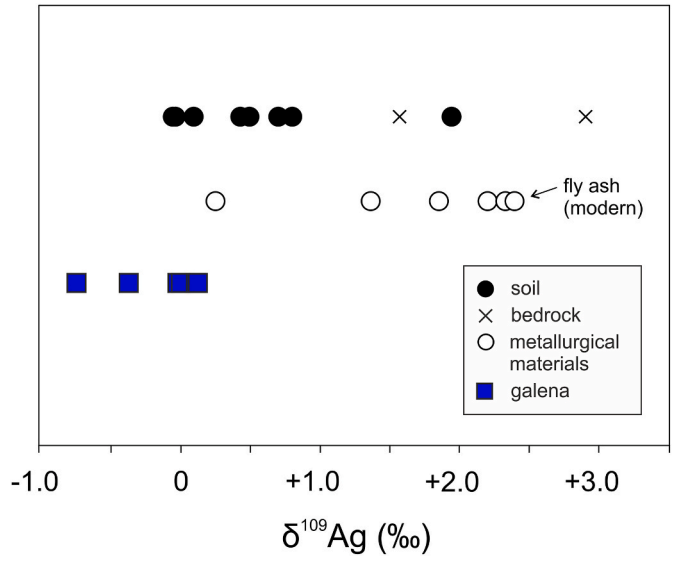

Fig. 1. Silver isotope variations (δ^{109}Ag) in the studied soil, bedrock, galena and metallurgical samples (slags, matte, fly ash). The δ^{109}Ag values are assigned an estimated error of ±0.10‰ (2σ) (see Silver isotope measurement).

during smelting (see the next paragraph). Considering the high melting and boiling points of Ag (962 and 2162 °C, respectively; Mango, 2018), the positive δ^{109}Ag values in the slags, or even the matte sample (72C) with +0.25‰, can only partially result from the high-T smelting process itself. One may hypothesize that the heavier ^{109}Ag isotope preferentially enters the slag phase, making the fly ash or vapor phases isotopically lighter. This isotopic pattern was demonstrated for Tl isotopes (^{203}Tl and ^{205}Tl) within our previous studies, dealing with industrial coal burning and secondary Zn roasting processes (Vaněk et al., 2016, 2018). It was concluded that fly ashes tend to concentrate the isotopically lighter Tl fraction compared to bottom ashes or slags (relatively enriched in ^{205}Tl). There is an analogy reported by Bigalke et al. (2010a) for Zn isotopes in fly ash (δ^{66}Zn, −0.41‰), as compared to heavier Zn observed in slag or solid waste derived from Cu smelting (0.18‰ and 0.25‰, respectively). Similarly, Kříbek et al. (2018) observed the variability of Cu isotopes among individual Cu-containing starting and waste materials within both Cu ore roasting/smelting processes. The authors even found that the emitted smelter dust was isotopically lighter (δ^{65}Cu, +0.15‰) than the isotopic composition of the respective smelter charges (≤+0.44‰). However, Gale et al. (1999), Mattielli et al. (2006) and Bigalke et al. (2010a,b) all concluded that, unlike Zn, Cu cannot fractionate during smelting processes, mainly because of its high boiling temperature (2562 °C), 400 °C higher than for Ag. Mathur et al. (2009) report that Cu ores and ore minerals generally show a wide range of Cu isotope ratios (δ^{65}Cu, ≤27 units), therefore being more important than the isotopic Cu fractionation during the high-T processes. As a result, the products of Cu smelting reflect the mineralogical differences in starting processed materials (Kříbek et al., 2018).

Combining all available knowledge, one could theoretically expect kinetic effects of Ag stable isotopes within individual metallurgical phases, i.e. between contrasting waste products such as the vapor phase, fly ash or slag. However, the degree of kinetically controlled Ag isotopic

fractionation, i.e. if it can be identified, is likely to be substantially lower than the isotopic variability of secondary metallurgical materials reflecting the isotopic composition of the initial Ag sources or changes in Ag binding and/or phase chemistry (Mathur et al, 2009, 2018).

As far as the speciation of Ag in modern fly ashes and historical emissions is concerned, the formation of Ag(I)S-like phases is reasonably inferred (Eckelman and Graedel, 2007). It should be noted that, with the exception of metallic Ag^0 in Ag-bearing PbS, Ag can be present as Ag(I) in various sulfides or complex sulfosalts, mostly forming the submicroscopic inclusions (Costagliola et al., 2003). In light of the affinity of Ag(I) to S, on the basis of thermodynamic and thermal stability data, β- and γ-Ag_2S polymorphs are assumed to prevail in smelter-derived flue gas/dust, as α-Ag_2S (acanthite) rapidly degrades at temperatures ≥179 °C (Sadovnikov and Vovkotrub, 2018). Unfortunately, we do not have direct evidence concerning the Ag speciation in our samples, since all the identified Ag concentrations are below the DLs suitable for a solid speciation analysis using EPMA or the XAS-based techniques.

3.2. Soil mineralogy, distribution and mobility of silver in soils

The mineralogical composition of soil profiles was dominated by quartz (SiO_2), K-feldspar ($KAlSi_3O_8$), Na-rich plagioclase ($NaAlSi_3O_8$) and muscovite ($KAl_2(AlSi_3O_{10})$ $(F,OH)_2$), followed by minor phases consisting of illite ($(K,H_3O)Al_2(Si,Al)_4O_{10}(OH)_2$) and chlorite ($(Mg,Al)_6(Si,Al)_4O_{10}(OH)_8$), as determined by the XRD in bulk and separated clay samples. Additionally, hematite (Fe_2O_3) and anglesite ($PbSO_4$) represented metalliferous phases detected in the heavily contaminated profile 2 (Table 2).

Comparable trends in Ag concentrations were observed in both profiles, which showed a peak in the subsurface horizon O2 (Fig. 2). This finding demonstrates the role of forest floor humus in the retention of Ag-rich dust particles, which is also consistent with maximum Pb and S soil concentrations. On the contrary, the lowest Ag concentrations were recorded in the bottom AC horizons which, in fact, are relatively richer in geogenic Ag (Table 2). The Ag concentration trends normalized by Ti (Table 2), being a conservative element depleted in industrial materials, support the anthropogenic input of Ag into the studied soils. In addition, the calculated τ parameter demonstrates a very high rate of the Ag enrichment, especially in the profile 2. It is important to highlight that no post-depositional interaction of soil organic matter and the smelter-derived Ag can be inferred from the chemical fractionation data. This is quite surprising, at least in respect of the low pH values (≤4 in the H_2O solution) and the organic nature of soil horizons (Table 1), which point to a tendency of acidic Ag leaching. However, the exchangeable and the oxalate-extractable Ag fractions in soils were extremely low, corresponding to ≤0.2% of total Ag contents. Therefore, the vast majority of soil Ag was apparently present in the residual fraction, associated with e.g., Ag-containing sulfides, sulfates and silicates. The XRD detection of anglesite ($PbSO_4$) in profile 2 (see Study area, soil sampling and characterization) further supports the suggestion that Ag is geochemically stable (insoluble) in our soils. By combining oxalate-extractable Fe and Mn data with the trends in exchangeable and oxalate-extractable Ag concentrations (≤50 μg Ag/kg) (Tables 1 and 2), it is implied that the degree of Ag adsorption to soil Fe/Mn-oxides or possibly to clay minerals was negligible (Jacobson et al., 2005a). Another implication of the conservative behavior of Ag is related to minimal migration of dissolved Ag species. Therefore, it is also possible to suppose that the prevailing mechanism of vertical Ag transport in soil profiles is particulate, i.e., via the smelter-derived (undissolved) dust particles.

3.3. Silver stable isotopes in soils

Both soil profiles exhibited markedly lighter Ag of metallurgical origin in the upper sections O1–O3, with $\delta^{109}Ag$ ranging between −0.05 and + 0.80‰ (Fig. 2). A comparison of the $\delta^{109}Ag$ values of these horizons with the signatures of the bottom AC horizons, including the

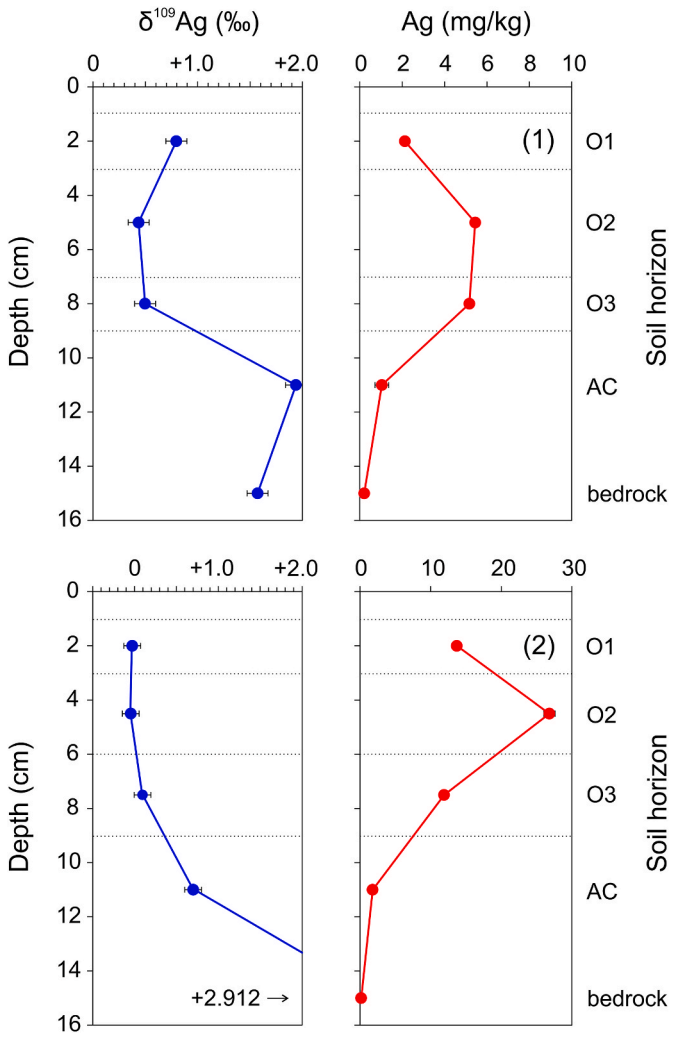

Fig. 2. Vertical evolution of Ag isotopic composition ($\delta^{109}Ag$) and total Ag concentration in the studied soil profiles – 1 and 2. The $\delta^{109}Ag$ values are assigned an estimated error of ±0.10‰ (2σ) (see Silver isotope measurement).

bedrocks, demonstrates that the latter is highly depleted of ^{107}Ag (≤+2.91‰) (Fig. 2). Considering no/limited solubility of Ag in the soils, the positive $\delta^{109}Ag$ values in the bottom horizons cannot reflect the isotopic fractionation of anthropogenic Ag, but only simply result from the introduction of geogenic Ag. Although, information about the controls affecting Ag isotope systematics in soil systems is not available in the literature, especially redox-driven interactions potentially represent the key factor, similar to other stable trace elements (e.g. Bigalke et al., 2010a,b; Mathur et al., 2018; Vejvodová et al., 2020).

Additional evidence for the anthropogenic origin of Ag in the upper profile sections is provided by inverse Ag concentrations (1/Ag) versus Ag isotopic data, as determined for all soil and bedrock samples (Fig. 3). Given the overall isotopic pattern, a three-component mixing of the two major anthropogenic Ag pools and a minor geogenic Ag pool can be inferred. In terms of calculating the contributions of each source, the following three linear equations and the associated matrix analysis (TERNARY_MIXING_MODEL.xlsx, Supplementary Material) were used as the model in this study (Equations (2)–(4)):

$$p_1 + p_2 + p_2 = 1 \quad (2)$$

$$\delta^{109}Ag_1 \times p_1 + \delta^{109}Ag_2 \times p_2 + \delta^{109}Ag_3 \times p_3 = \delta^{109}Ag_{soil} \quad (3)$$

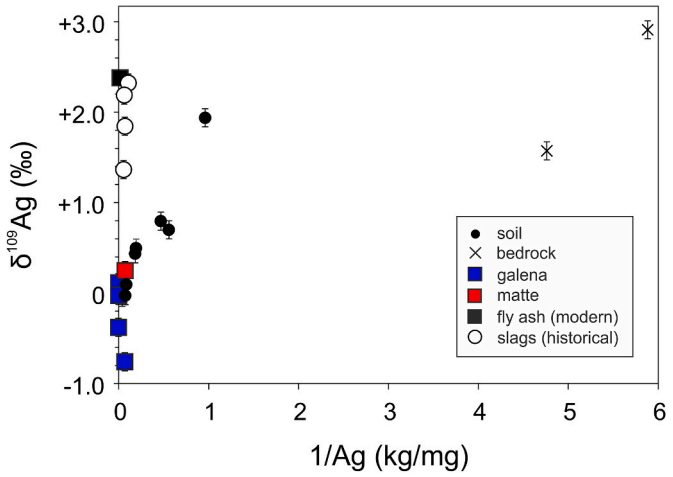

Fig. 3. Silver isotopic compositions (δ^{109}Ag) versus 1/Ag concentrations in the studied soil, bedrock, galena and metallurgical samples. The δ^{109}Ag values are assigned an estimated error of ±0.10‰ (2σ) (see Silver isotope measurement).

$$\frac{p_1 \times C_{soil}}{C_1} + \frac{p_2 \times C_{soil}}{C_2} + \frac{p_3 \times C_{soil}}{C_3} = 1 \quad (4)$$

where p_i represents relative source contributions (3 unknowns) and $\delta^{109}Ag_i$ and C_i indicate Ag isotopic signatures and Ag concentrations of individual endmembers and the soil sample.

When viewing the Ag isotopic signatures of individual ore and metallurgical samples, a combination of galena and slag data shows the best match with the contaminated soils (Fig. 3). The modern fly ash sample from battery processing could not be used as a valid Ag endmember since it does not cover the long history of Ag contamination caused by local ore processing. Assuming that the Ag occurring in the profiles is an isotopic mixture of anthropogenic Ag and geogenic Ag as for bedrocks (δ^{109}Ag +1.57 and + 2.91‰) (Fig. 1), the calculated smelter-derived Ag load corresponds to a minimum of 90% of the total amount of soil Ag. This type of mixing model allow us to virtually interpret why the anthropogenic $^{109}Ag/^{107}Ag$ signal is somewhat shifted (≤0.8 δ^{109}Ag) between the profiles (1 and 2) (Fig. 2). In other words, variations of Ag sources (and emission loads) with varying isotopic compositions at the two sampling sites (Fig. S1) may offer a reasonable explanation as to why the isotopic composition of Ag is variable.

In order to quantify the overall addition of anthropogenic Ag in the soils, relative to the unaltered bedrocks, we used the τ-parameter. This approach enables to identify the proportion of Ag gained or eventually lost at a specific soil horizon, relative to an immobile (conservative) Ti (Eq. (5)).

$$\tau_{Ag/Ti} = \frac{(C_{Ag}/C_{Ti})_{soil}}{(C_{Ag}/C_{Ti})_{bedrock}} - 1 \quad (5)$$

Where C are the concentrations of Ag and Ti in the soil or bedrock samples. Since the calculated τ values have a wide range and are mostly very high (1–260) (Table 2), it is clear that most soil horizons are extremely enriched in anthropogenic Ag, which is consistent with the isotopic data.

Regarding the positive δ^{109}Ag values in the bedrocks, a combination of the τ, Pb concentration and δ^{109}Ag soil data favors Ag and Pb relationships, suggesting that isotopically heavy sulfides (and silicates) are present in native soils (Fig. 4a and b), meaning that the soils are getting heavy Ag from distal Ag mineralization. Since both bedrocks have very low Ag contents (≤0.2 mg/kg), their isotopic signal can only reflect important changes in Ag mineralogy, i.e. consisting of Ag-poor phases that are simultaneously highly δ^{109}Ag positive (Figs. 1 and 2). Clearly, more rock and deep soil sampling will be required in the future to confirm the theory of different Ag isotope signatures in the host rocks in the studied geological terrain.

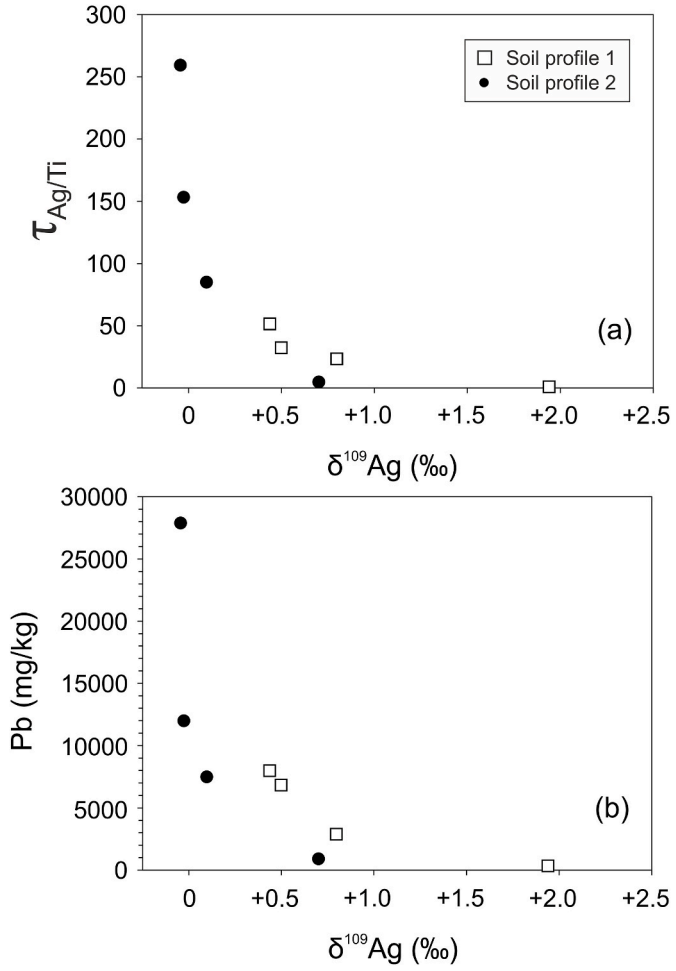

Fig. 4. a,b. Variations in the τ-value and the Pb concentration versus δ^{109}Ag data in the studied soils.

4. Conclusions

In this study, we demonstrate that Ag isotope ratios can significantly vary in both primary ore and secondary metallurgical materials (galena, fly ash, slag and matte). This phenomenon, however, is not necessarily representative of how, or to what degree the material is subjected to the Ag isotopic fractionation, but it is mainly inherited from the starting $^{109}Ag/^{107}Ag$ signal in ore mineral or specific type of ore genesis. Therefore, we assume that the Ag isotopes have a promising potential to trace phase changes or to monitor specific geochemical processes. Our data also demonstrate that historical Ag contamination of soil systems can be traced and even quantified using Ag isotope ratios. Accordingly, we did not observe any post-depositional isotopic fractionation(s) in the studied soils, since Ag was geochemically stable and was not subjected to leaching.

To gain further insights into the Ag dynamics in surface environments and the processes that can affect Ag isotopic patterns in soils, model studies are required to determine the fractionation factors for individual chemical processes. From this viewpoint, redox reactions presumably play the key role that can be identifiable using Ag isotopic ratios as proxies.

Author statement

Vaněk Aleš: Concept, Methodology, Data Processing, Paper Preparation/Editing. Maria Vaňková: Isotopic Analyses, Data Processing, Paper Editing. Martin Mihaljevič: Isotopic Analyses, Paper Editing. Vojtěch Ettler: Partial Data Interpretations, Paper Editing. Petr Drahota: Mineralogical Analyses, Paper Editing. Lenka Vondrovicová: Isotopic Analyses. Petra Vokurková: Soil Analyses. Ivana Galušková: Soil Analyses. Tereza Zádorová: Partial Data Interpretations. Ryan Mathur: Concept, Data Processing, Paper Editing.

Declaration of competing interest

The authors declare that they have no known competing financial interests or personal relationships that could have appeared to influence the work reported in this paper.

Data availability

Data will be made available on request.

Acknowledgements

This research was funded by the grant of the Czech Science Foundation (23-04891S). Marie Fayadová is thanked for her laboratory assistance. The three anonymous reviewers are acknowledged for all the helpful comments and suggestions that improved the quality of the original manuscript version.

Appendix A. Supplementary data

Supplementary data to this article can be found online at https://doi.org/10.1016/j.envpol.2023.122557.

References

Albarède, F., Blichert-Toft, J., Rivoal, M., Telouk, P., 2016. A glimpse into the Roman finances of the Second Punic War through silver isotopes. Geochemical Perspective Letters 2, 127–137. https://doi.org/10.7185/geochemlet.1613.

Anderson, C.J., Mathur, R., Rakovan, J., Tremsin, A.S., 2019. Natural solid-state ion conduction induces metal isotope fractionation. Geology 47, 617–621. https://doi.org/10.1130/G45999.1.

Arribas, A., Mathur, R., Megaw, P., Arribas, I., 2020. The isotopic composition of silver in ore minerals. G-cubed 21, e2020GC009097. https://doi.org/10.1029/2020GC009097.

Ash, C., Borůvka, L., Tejnecký, V., Nikodem, A., Šebek, O., Drábek, O., 2014. Potentially toxic element distribution in soils from the Ag-smelting slag of Kutná Hora (Czech Republic): descriptive and prediction analyses. J. Geochem. Explor. 144, 328–336. https://doi.org/10.1016/j.gexplo.2013.11.010.

Bigalke, M., Weyer, S., Kobza, J., Wilcke, W., 2010a. Stable Cu and Zn isotope ratios as tracers of sources and transport of Cu and Zn in contaminated soil. Geochem. Cosmochim. Acta 74, 6801–6813. https://doi.org/10.1016/j.gca.2010.08.044.

Bigalke, M., Weyer, S., Wilcke, W., 2010b. Stable copper isotopes: a novel tool to trace copper behavior in hydromorphic soils. Soil Sci. Soc. Am. J. 74, 60–73. https://doi.org/10.2136/sssaj2008.0377.

Costagliola, P., Di Bendedetto, F., Benvenuti, M., Bernardini, G.P., Cipriani, C., Lattanzi, P., Romanelli, M., 2003. Chemical speciation of Ag in galena by EPR spectroscopy. Am. Mineral. 88, 1345–1350. https://doi.org/10.2138/am-2003-8-918.

Desaulty, A.-M., Telouk, P., Albalat, E., Albarède, F., 2011. Isotopic Ag–Cu–Pb record of silver circulation through 16th–18th century Spain. Proc. Natl. Acad. Sci. U.S.A. 108, 9002–9007. https://doi.org/10.1073/pnas.1018210108.

Desaulty, A.-M., Albarède, F., 2013. Copper, lead, and silver isotopes solve a major economic conundrum of Tudor and early Stuart Europe. Geology 41, 135–138. https://doi.org/10.1130/G33555.1.

Eshel, T., Tirosh, O., Yahalom-Mack, N., Gilboa, A., Erel, Y., 2022. Silver isotopes in silver suggest Phoenician innovation in metal production. Apllied Sciences 12, 741. https://doi.org/10.3390/app12020741.

Ettler, V., Legendre, O., Bodénan, F., Touray, J.C., 2001. Primary phases and natural weathering of old lead-zinc pyrometallurgical slag from Příbram, Czech Republic. Can. Mineral. 39, 873–888. https://doi.org/10.2113/gscanmin.39.3.873.

Ettler, V., Piantone, P., Touray, J.-C., 2003. Mineralogical control on inorganic contaminant mobility in leachate from lead-zinc metallurgical slag: experimental approach and long-term assessment. Mineral. Mag. 67, 1269–1283. https://doi.org/10.1180/0026461036760164.

Ettler, V., Mihaljevič, M., Komárek, M., 2004. ICP-MS measurements of lead isotopes in soils heavily contaminated by lead smelting: tracing the sources of pollution. Anal. Bioanal. Chem. 378, 311–317. https://doi.org/10.1007/s00216-003-2229-y.

Ettler, V., Vaněk, A., Mihaljevič, M., Bezdička, P., 2005a. Contrasting lead speciation in forest and tilled soils heavily polluted by lead metallurgy. Chemosphere 58, 1449–1459. https://doi.org/10.1016/j.chemosphere.2004.09.084.

Ettler, V., Johan, Z., Baronnet, A., Jankovský, F., Gilles, C., Mihaljevič, M., Šebek, O., Strnad, L., Bezdička, P., 2005b. Mineralogy of air-pollution-control residues from a secondary lead smelter: environmental implications. Environ. Sci. Technol. 39, 9309–9316. https://doi.org/10.1021/es0509174.

Ettler, V., Červinka, R., Johan, Z., 2009a. Mineralogy of medieval slags from lead and silver smelting (Bohutín, Příbram district, Czech Republic): towards estimation of historical smelting conditions. Archaeometry 51, 987–1007. https://doi.org/10.1111/j.1475-4754.2008.00455.x.

Ettler, V., Johan, Z., Bezdička, P., Drábek, M., Šebek, O., 2009b. Crystallization sequences in matte and speiss from primary lead metallurgy. Eur. J. Mineral 21, 837–854. https://doi.org/10.1127/0935-1221/2009/0021-1942.

Fabrega, J., Luoma, S.N., Tyler, C.R., Galloway, T.S., Lead, J.R., 2011. Silver nanoparticles: behavior and effects in the aquatic environment. Environ. Int. 37, 517–531. https://doi.org/10.1016/j.envint.2010.10.012.

Fujii, T., Albarede, F., 2018. ^{109}Ag–^{107}Ag fractionation in fluids with applications to ore deposits, archeometry, and cosmochemistry. Geochem. Cosmochim. Acta 234, 37–49. https://doi.org/10.1016/j.gca.2018.05.013.

Gale, N.H., Woodhead, A.P., Stos-Gale, Z.A., Walder, A., Bowen, I., 1999. Natural variations detected in the isotopic composition of copper: possible applications to archaeology and geochemistry. Int. J. Mass Spectrom. 184, 1–9. https://doi.org/10.1016/S1387-3806(98)14294-X.

Gee, G.W., Bauder, J.W., 1986. Particle-size analysis. In: Klute, A. (Ed.), Methods of Soil Analysis, Part I: Physical and Mineralogical Methods. American Society of Agronomy-Soil Science Society of America, Madison, WI, pp. 383–412.

Guo, Q., Wei, H.-Z., Jiang, S.-Y., Hohl, S., Lin, Y.-B., Wang, Y.-J., Li, Y.-C., 2017. Matrix effects originating from coexisting minerals and accurate determination of stable silver isotopes in silver deposits. Anal. Chem. 89, 13634–13641. https://doi.org/10.1021/acs.analchem.7b04212.

Jacobson, A.R., McBride, M.B., Baveye, P., Steenhuis, T.S., 2005a. Environmental factors determining the trace-level sorption of silver and thallium to soils. Sci. Total Environ. 345, 191–205. https://doi.org/10.1016/j.scitotenv.2004.10.027.

Jacobson, A.R., Klitzke, S., McBride, M.B., Baveye, P., Steenhuis, T.S., 2005b. The desorption of silver and thallium from soils in the presence of a chelating resin with thiol functional groups. Water Air Soil Pollut. 160, 41–54. https://doi.org/10.1007/s11270-005-3860-3.

Kříbek, B., Šípková, A., Ettler, V., Mihaljevič, M., Majer, V., Knésl, I., Mapani, B., Penížek, V., Vaněk, A., Sracek, O., 2018. Variability of the copper isotopic composition in soil and grass affected by mining and smelting in Tsumeb, Namibia. Chem. Geol. 493, 121–135. https://doi.org/10.1016/j.chemgeo.2018.05.035.

Kunický, Z., Vurm, K., 2011. 700 Let Hutnictví Stříbra a Olova Na Příbramsku (In Czech); Kovohutě Příbram Nástupnická a. S. Příbram, Czech Rep.

Lu, D., Liu, Q., Zhang, T., Cai, Y., Yin, Y., Jiang, G., 2016. Stable silver isotope fractionation in the natural transformation process of silver nanoparticles. Nat. Nanotechnol. 11, 682–686. https://doi.org/10.1038/nnano.2016.93.

Luo, Y., Dabek-Zlotorzynska, E., Celo, V., Muir, D.C.G., Yang, L., 2010. Accurate and Precise Determination of silver isotope fractionation in environmental samples by multicollector-ICPMS. Anal. Chem. 82, 3922–3928. https://doi.org/10.1021/ac100532r.

Mango, H., 2018. Silver. In: White, W.M. (Ed.), Encyclopedia of Geochemistry. Encyclopedia of Earth Sciences Series. Springer, Cham, Switzerland, pp. 1340–1344. https://doi.org/10.1007/978-3-319-39312-4_257.

Mathur, R., Titley, S., Barra, F., Brantley, S., Wilson, M., Phillips, A., Munizaga, F., Maksaev, V., Vervoort, J., Hart, G., 2009. Exploration potential of Cu isotope fractionation in porphyry copper deposits. J. Geochem. Explor. 102, 1–6. https://doi.org/10.1016/j.gexplo.2008.09.004.

Mathur, R., Arribas, A., Megaw, P., Wilson, M., Stroup, S., Meyer-Arrivillaga, D., Arribas, I., 2018. Fractionation of silver isotopes in native silver explained by redox reactions. Geochem. Cosmochim. Acta 224, 313–326. https://doi.org/10.1016/j.gca.2018.01.011.

Mattielli, N., Rimetz, J., Petit, J., Perdrix, E., Deboudt, K., Flament, P., Weis, D., 2006. Zn-Cu isotopic study and speciation of airborne metal particles within a 5-km zone of a lead zinc smelter. Geochem. Cosmochim. Acta 70, A401. https://doi.org/10.1016/j.gca.2006.06.808.

Milot, J., Blichert-Toft, J., Sanz, M.A., Malod-Dognin, C., Télouk, P., Albarède, F., 2022. Silver isotope and volatile trace element systematics in galena samples from the Iberian Peninsula and the quest for silver sources of Roman coinage. Geology 50, 422–426. https://doi.org/10.1130/G49690.1.

Nakajima, K., Takeda, O., Miki, T., Matsubae, K., Nakamura, S., Nagasaka, T., 2010. Thermodynamic analysis of contamination by alloying elements in aluminum recycling. Environ. Sci. Technol. 44, 5594–5600. https://doi.org/10.1021/es9038769.

Nakajima, K., Takeda, O., Miki, T., Matsubae, K., Nagasaka, T., 2011. Thermodynamic analysis for the controllability of elements in the recycling process of metals. Environ. Sci. Technol. 45, 4929–4936. https://doi.org/10.1021/es104231n.

Nowack, B., Krug, H.F., Height, M., 2011. 120 years of nanosilver history: implications for policy makers. Environ. Sci. Technol. 45, 1177–1183. https://doi.org/10.1021/es103316q.

Pansu, M., Gautheyrou, J., 2006. Handbook of Soil Analysis: Mineralogical, Organic and Inorganic Methods. Springer-Verlag, Berlin, Heidelberg, Germany.

Pei, Y., Chen, X., Xiong, D., Liao, S., Wang, G., 2013. Removal and recovery of toxic silver ion using deep-sea bacterial generated biogenic manganese oxides. PLoS One 8, e81627. https://doi.org/10.1371/journal.pone.0081627.

Purcell, T.W., Peters, J.J., 1998. Sources of silver in the environment. Environ. Toxicol. Chem. 17, 539–546. https://doi.org/10.1002/etc.5620170404.

Reimann, C., Fabian, K., 2022. Quantifying diffuse contamination: comparing silver and mercury in organogenic and minerogenic soil. Sci. Total Environ. 832, 155065 https://doi.org/10.1016/j.scitotenv.2022.155065.

Rieuwerts, J.S., Farago, M., Cikrt, M., Bencko, V., 1999. Heavy metal concentrations in and around households near a secondary lead smelter. Environ. Monit. Assess. 58, 317–335. https://doi.org/10.1023/A:1006058331453.

Sadovnikov, S.I., Vovkotrub, E.G., 2018. Thermal stability of nanoparticle size and phase composition of nanostructured Ag_2S silver sulfide. J. Alloys Compd. 766, 140–148. https://doi.org/10.1016/j.jallcom.2018.06.351.

Scheinert, M., Kupsch, H., Bletz, B., 2009. Geochemical investigations of slags from the historical smelting in Freiberg, Erzgebirge (Germany). Chem. Erde 69, 81–90. https://doi.org/10.1016/j.chemer.2008.03.001.

Schönbachler, M., Carlson, R.W., Horan, M.F., Mock, T.D., Hauri, E.H., 2007. High precision Ag isotope measurements in geologic materials by multiple-collector ICPMS: an evaluation of dry versus wet plasma. Int. J. Mass Spectrom. 261, 183–191. https://doi.org/10.1016/j.ijms.2006.09.016.

Schönbachler, M., Carlson, R.W., Horan, M.F., Mock, T.D., Hauri, E.H., 2008. Silver isotope variations in chondrites: volatile depletion and the initial ^{107}Pd abundance of the solar system. Geochem. Cosmochim. Acta 72, 5330–5341. https://doi.org/10.1016/j.gca.2008.07.032.

Settimio, L., McLaughlin, M.J., Kirby, J.K., Langdon, K.A., Janik, L., Smith, S., 2015. Complexation of silver and dissolved organic matter in soil water extracts. Environ. Pollut. 199, 174–184. https://doi.org/10.1016/j.envpol.2015.01.027.

Standard of Soil Quality, 1994. Determination of Effective Cation Exchange Capacity and Base Saturation Level Using Barium Chloride Solution. ISO 11260:1994. International Organization of Standardization, Geneva. https://www.iso.org/standard/19238.html.

Standard of Soil Quality, 2009. Extraction of Trace Elements Form Soil Using Ammonium Nitrate Solution. ISO 19730:2008. Beuth Verlag, Berlin. https://www.beuth.de/de/norm/din-iso-19730/117095524.

Taylor, S.R., McLennan, S.M., 1985. The Continental Crust: its Composition and Evolution. Blackwell, Oxford.

Vaněk, A., Grösslová, Z., Mihaljevič, M., Trubač, J., Ettler, V., Teper, L., Cabala, J., Rohovec, J., Zádorová, T., Penížek, V., Pavlů, L., Holubík, O., Němeček, K., Houška, J., Drábek, O., Ash, C., 2016. Isotopic tracing of thallium contamination in soils affected by emissions from coal-fired power plants. Environ. Sci. Technol. 50, 9864–9871. https://doi.org/10.1021/acs.est.6b01751.

Vaněk, A., Grösslová, Z., Mihaljevič, M., Ettler, V., Trubač, J., Chrastný, V., Penížek, V., Teper, L., Cabala, J., Voegelin, A., Zádorová, T., Oborná, V., Drábek, O., Holubík, O., Houška, J., Pavlů, L., Ash, C., 2018. Thallium isotopes in metallurgical wastes/contaminated soils: a novel tool to trace metal source and behavior. J. Hazard Mater. 343, 78–85. https://doi.org/10.1016/j.jhazmat.2017.09.020.

Vejvodová, K., Vaněk, A., Mihaljevič, M., Ettler, V., Trubač, J., Vaňková, M., Drahota, P., Vokurková, P., Penížek, V., Zádorová, T., Tejnecký, V., Pavlů, L., Drábek, O., 2020. Thallium isotopic fractionation in soil: the key controls. Environ. Pollut. 265, 114822 https://doi.org/10.1016/j.envpol.2020.114822.

Wang, D., Mathur, R., Zheng, Y., Wu, H., Lv, Y., Zhang, G., Huan, R., Yu, M., Li, Y., 2022. Constraints on ore-forming fluid evolution and guidance for ore exploration in the Zhaxikang Sb-Pb-Zn-Ag deposit in southern Tibet: insights from silver isotope fractionation of galena. Miner. Deposita 57, 701–724. https://doi.org/10.1007/s00126-022-01111-5.

Woodland, S.J., Rehkämper, M., Halliday, A.N., Lee, D.C., Hattendorf, B., Günther, D., 2005. Accurate measurement of silver isotopic compositions in geological materials including low Pd/Ag meteorites. Geochem. Cosmochim. Acta 69, 2153–2163. https://doi.org/10.1016/j.gca.2004.10.012.

World Reference Base for Soil Resources, 2006. A Framework for International Classification, Correlation and Communication. Food and Agriculture Organization of the United Nations (FAO), Rome, Italy. https://www.fao.org/3/a0510e/a0510e.pdf.

Zhang, T., Lu, D., Zeng, L., Yin, Y., He, Y., Liu, Q., Jiang, G., 2017. Role of secondary particle formation in the persistence of silver nanoparticles in humic acid containing water under light irradiation. Environ. Sci. Technol. 51, 14164–14172. https://doi.org/10.1021/acs.est.7b04115.